Automatic detection of impact craters on Mars using a modified adaboosting method

Shuanggen Jin [a,*], Tengyu Zhang [a,b]

[a] Shanghai Astronomical Observatory, Chinese Academy of Sciences, Shanghai 200030, China
[b] University of Chinese Academy of Sciences, Beijing 100049, China

ARTICLE INFO

ABSTRACT

The accurate recognition of impact craters is important to analyze and understand the relative dating of Martian surface. Since manually identifying small craters in a deluge of high-resolution Martian images is a tremendous task, a robust automatic detection algorithm of the crater is needed, but subject to lots of uncertainties and low successful detection rates. In this paper, a modified adaboosting approach is developed to detect small size craters on Mars. First, we construct a dual-threshold weak classifier based on the characteristics of the feature value distribution instead of the single threshold classifier. Second, we adjust the criterion of updating weights in the process of training. The small craters on Mars are automatically detected based on the modified algorithm using the images from the High Resolution Stereo Camera (HRSC) onboard Mars Express with a resolution of 12.5 m/pixel. A high threshold with 0.85 is determined, and the true detection rate of small size craters on Mars is improved by almost 10% when compared to the original method. The true detection rate can be obtained as high as 85% with only 10% false detection rate. Therefore, the modified adaboosting method has greatly improved the detecting performance of the crater and reduced the detection time.

© 2014 Elsevier Ltd. All rights reserved.

1. Introduction

Impact craters are among the most noticeable geomorphological features on the planetary surface (e.g., Jin et al., 2013). It is important to detect and analyze the size frequency distribution because it is the only tool to survey the relative age of the geologic formation on the planetary surface (Crater Analysis Techniques Working Group, 1979). The criterion is simple that the heavily cratered surface is considered to be relatively older than the less cratered surface. According to previous research (Tanaka, 1986), the size frequency distribution of craters are always assumed to be approximated by the power law. Crater counting is a common and paramount approach for the planetary surface analysis. Many databases were built by means of visual inspection of images, which are spatially comprehensive but contain only the larger craters over the whole Mars (Barlow, 1988; Rodionova et al., 2000). Furthermore, it is a really time-consuming and laborious work to manually build a comprehensive crater catalog (Robbins and Hynek, 2012), and therefore it is necessary to develop an automatic crater detection algorithm to recognize the crater. Although a number of crater detection algorithms (CDA) have been

proposed (Salamuniccar and Loncaric, 2012), but they did not satisfy the high precise requirement due to the lack of great identification ability. In particular, with a wide range of craters size (from a few meters to thousands of kilometers), the craters on the planetary surface were normally determined by the degree of the degradation, internal morphologies and the degree of overlapping with other craters. Most craters have distinct conservation conditions varying from fresh state to old appearance with seriously eroded rims, which is a real challenge for the identification of craters from other geomorphologies. In addition, the diverse geomorphological settings and image illumination conditions make it more difficult to discriminate, even with visual inspection.

On the Martian surface, there are always rare large craters but abundant small craters. Previous crater catalogs of large craters on a global scale were constructed by visual inspection (Andersson and Whitaker, 1982; Kozlova et al., 2001), but it took a huge work load. For example, the most comprehensive crater catalogs were built by Barlow (1988) and Salamuniccar and Loncaric (2008a), which contained 42,283 craters and 57,633 craters with diameter of larger than 5 km. Most of them focused on the detection of craters with large size on areas without complex geomorphological features, but sometimes it was not precise enough to be landmarks for spacecraft in autonomous navigation (Leroy et al., 2001). With increasing demands of the smaller craters detection on more complex

planetary surface conditions, millions of smaller craters on Martian surface are waiting to be identified from images at higher and higher spatial resolution.

There are two general kinds of the automatic detection methods: supervised and unsupervised approaches (Stepinski et al., 2009; Ding et al., 2011; Troglio et al., 2012). Many unsupervised algorithms are based on pattern recognition techniques and crater rims are identified as circular objects in an image (Leroy et al., 2001; Kim and Muller, 2003; Bandeira et al., 2007). The machine learning technique, training of classifiers for discriminating craters from non-craters, is utilized in supervised approaches. The unsupervised algorithms are always fully autonomous but less accurate than supervised approaches. In addition, most previous studies based on the unsupervised algorithms relied on the inefficient pixel-based approaches, which may detect some large craters but have low possibility to detect small craters from high resolution planetary image with billions of pixels. The supervised algorithms are normally feature-based approaches, which require a set of well-chosen features and effective criteria with high discriminative power. From previous researches, no hand-made or defined patterns can make a big difference in distinguishing craters from non-craters. Therefore, machine-learning algorithms are useful for crater detection (Wetzler et al., 2005).

An unsupervised method, template matching of probability volume, was introduced for the recognition of impact craters (Bandeira et al., 2007), which was employed in the detection of craters on Mars Orbiter Camera images. Based on the characteristic shapes of craters, it was proposed that small craters can be detected efficiently (Urbach and Stepinski, 2009). The detection percentage is about 70%, which is not enough for detecting small craters. To avoid some disadvantages of optical images, an approach based on DEM data was presented by Bue and Stepinski (2007), but it has a worse performance in the recognition of craters. Currently, the effective algorithm, Adaptive Boosting, has been well used in automatically detecting craters (Martins et al., 2009; Ding et al., 2011; Bandeira et al., 2012), but it still has some limitations in detection efficiency and small size craters. In this paper, a modified adaboosting approach is developed to detect small size craters on Mars, which is aimed at improving the performance and efficiency of detecting craters. In Section 2, the algorithm and method are presented, Section 3 shows the test results, and finally conclusions and future works are given in Section 4.

2. Algorithms and methods

The traditional algorithm was first introduced in the detection of craters by Martins et al. (2009), which was used in the field of face recognition (Viola and Jones, 2004). It is a boosting algorithm that relies on the strong classifier with a sequence of weak classifiers to discriminate craters from non-craters.

2.1. Crater and non-crater candidates

The algorithm of the craters detection is a machine-learning algorithm, which needs to select candidates for machine learning in the training process. The face training set can be extracted randomly from the face dataset, which are direct and useful samples for classification between face and non-face images (Viola and Jones, 2004). However, no complete dataset can be used for the selection of crater candidates. Moreover, the crater appearance on the image results from illumination angle, surface properties and atmospheric state, which may result in that the feature of craters from one type of images cannot well represent the craters from another type. Therefore, we should make sure that the image block of candidates has the same image quality with the test image. Therefore the

candidate images and the test images are of the same data source from the High Resolution Stereo Camera (HRSC) onboard Mars Express. Each crater candidate is a square image block with a fixed size, whose width can be set with a dimension of the same as the diameter of the crater. All the candidates will be extracted from the overall image with more than tens of thousands craters in the entire scene in order to have best ability to discriminate craters and non-craters in the image. Considering the variability of craters shapes, 400 crater candidates and 400 non-crater candidates are chosen in the training process.

First tens of crater and non-crater candidates are manually selected from the test area image as the input data for this machine learning algorithm, which can be easily done with visual identification. To avoid too much false detections, the relatively large threshold value will be used in the algorithm. After quickly scanning the image, enough image blocks with positive and negative detections will be obtained so that candidates are with the same image quality as the test area.

2.2. Haar-like feature extraction

The Haar basis functions were first proposed for the detection of objects (Papageorgiou et al., 1998) and then popularized in the context of fast face recognition, which were the fundamental and vital part for our feature extraction. The features are built by using a family of binary masks, whose numerical values are calculated as an attribution to distinguish craters from non-craters. The Haar-like features are different kinds of rectangular regions with various sizes and consisted of two kinds of sectors (white sector and black sector). By setting the feature mask in the prepared image block, we can obtain the feature value by subtracting the sum of grayscale values of the pixels covered by the white sector from the sum of grayscale values of the black sector. A mask is scanned within the region of a crater candidate in different scales. Thus more than 60,000 features will be assembled in a mask with 24×24 pixel by an arrangement of the sectors and placement within an image block. These features are over-complete and even redundant for the classification between craters and non-craters objects. The craters with circular shapes are always identified in a symmetric pattern. In order to reduce the computational complexity, we use only square mask-features because in general we are aimed to detect round craters characterized by their distinct rims.

According to Martins et al. (2009), 10 types of mask-features are used in this algorithm with different patterns in Fig. 1. For the implementation of extracting the features from the candidates, all of the candidates will be resized to a standardized size of 24×24 pixel, which is the smallest size that we can detect in the tested image. For the first nine features in Fig. 1, four different sizes are used, i.e., 6×6, 12×12, 18×18 and 24×24, respectively. Each is separated by a third of mask size. Then there are 1089 features for each candidate of these nine patterns. The last feature is based on the circular shape of craters. 324 more features will be added when the side lengths of the two inside squares vary with a step size of 2 pixel.

2.3. Feature selection and classification

Given a set of features and a training set of crater and non-crater candidates, a number of weak classifier can be built to classify candidates into craters and non-craters. The main steps of the traditional algorithm are briefly described as the following:

1) Initialize weights $w_{1,i} = (1/2m)$, $(1/2n)$, where m and n are the number of craters and non-craters in the training set, respectively;
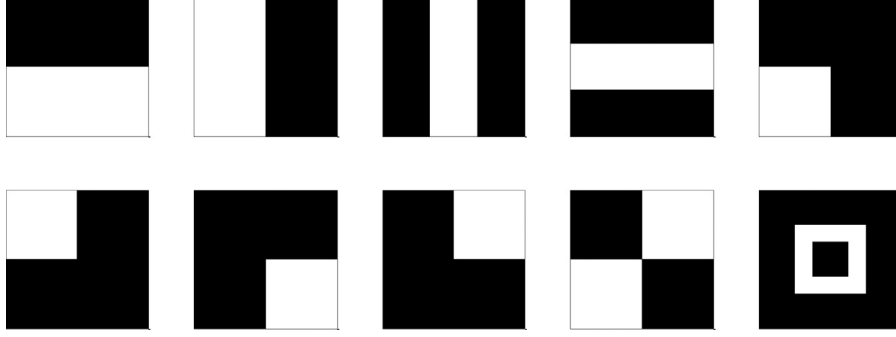
Fig. 1. Ten types of mask-features.

2) For $t = 1$ to T, where T is a desired number of most discriminative weak classifiers;
3) Normalize the weights, $w_{t,i} = w_{t,i} / \sum_{j=1}^{m+n} w_{t,j}$;
4) For all the used features, the weak classifier is selected with satisfying the criterion of minimum weighted classification errors as $\varepsilon_t = \min_{f,p,\theta} \sum_i w_{t,i} |h(C_i, f, p, \theta) - c_i|$, where $c_i = 0$ or 1 for craters and non-craters examples, respectively, and $h_t(C) = h(C, f_t, p_t, \theta_t)$ is a weak classifier that will be discussed in details later;
5) Update the weights, $w_{t+1,i} = w_{t,i} \beta_t^{1-e_i}$, where $e_i = 0$ if the candidate is classified correctly, and $e_i = 1$ if the candidate is classified incorrectly, where $\beta_t = \varepsilon_t / (1 - \varepsilon_t)$;
6) End;
7) The final strong classifier is given by:

$$H(C) = \begin{cases} \text{crater} & \text{if } \sum_{t=1}^{T} \alpha_t \times h_t(C) > \mu \times \sum_{t=1}^{T} \alpha_t \\ \text{non} - \text{crater} & \text{otherwise} \end{cases},$$

where $\alpha_t = \log(1/\beta_t)$ and μ is a threshold probability.

2.4. The modified weak classifier

In the traditional algorithm, a sequence of weak classifiers was generated and combined to assemble a strong classifier through a weighted boosting approach. A set of weak classifiers $h_t(C) = h(C, f_t, p_t, \theta_t)$ is defined as:

$$h(C; f, p, \theta) = \begin{cases} 1 & \text{if } p \times f(C) \geq p \times \theta \\ 0 & \text{else} \end{cases} \qquad (1)$$

where C is an image block representing a crater candidate and f is the numeric value of each feature. The discriminative power of the weak classifier is determined by the threshold θ and a polarity variable $p \in \{1, -1\}$, which means that the feature value should be larger or smaller than the threshold. In fact, each single weak classifier always identifies candidates into craters with a low confidence because of its low discriminative power. However, in each round of the training process a best weak classifier will be selected with the minimum weighted errors. If all these weak classifier has an ability of correct classification with a detection rate of higher than 0.5, the final strong classifier can perform well by combining many weak classifiers.

Fig. 2 shows the proportion of crater and non-crater candidates in all candidates when the feature value increases. Considering the distribution of the sum weight of all the candidates, we can conclude that the feature value of crater candidates distributes in a relatively narrow interval when compared to non-crater candidates. Only a single side threshold to determine craters will result in some false results, like the non-crater candidates with very high or low features. Therefore, the classifier with a dual-threshold is constructed for the detection. It can be easily
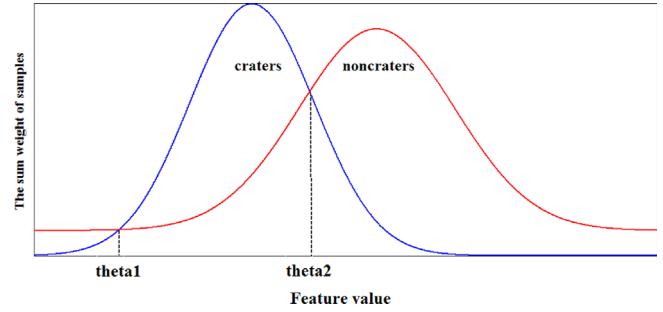

Fig. 2. The distribution of the sum weight of the candidates.

proved that smaller classification errors will be obtained when a weak classifier with a dual-threshold is employed, which is introduced in the following:

$$h(C; f, \theta_1, \theta_2) = \begin{cases} 1 & \text{if } \theta_1 \leq f(C) < \theta_2 \\ 0 & \text{else} \end{cases} \qquad (2)$$

therefore we should find these two thresholds in the next step, as the following:

1) According to the distribution range of the numeric value of the features, we will divide the ranges into some intervals to calculate the sum weight of craters $g(x)$ and non-craters $ng(x)$;
2) For each interval x_i, we can subtract $ng(x)$ from $g(x)$ and get $h(x) = g(x) - ng(x)$;
3) After obtaining the value of max $(h(x))$, the x_{max} corresponding to $h(x)_{max}$ can be found. On the left and right side of x_{max}, x_1 and x_2 can be got to satisfy the equation: $h(x) = 0$. In fact, the function $h(x)$ is not continuous, so the requirement cannot be satisfied strictly. Therefore, the value of x will be selected when $h(x)$ vary from the negative to the positive or the positive to the negative. The classification errors can be minimized when we use x_1 and x_2 as two thresholds.

2.5. Weight updating

According to the method of updating weights proposed in AdaBoost (Freund and Schapire, 1995), the weights of incorrectly classified candidates are increased and the weights of correctly classified candidates are decreased so that incorrectly classified examples will be of greater possibility to be chosen for calculating the sum weighted error in the next iteration. Now it has been popularly used in crater detection algorithms (Martins et al., 2009; Ding et al., 2011; Bandeira et al., 2012). However, when the examples are correctly classified, they are not given enough weighs in the weights updating process. To bring down the rate

of false or negative detection, we adjust with the weight factor α_t so that the weak classifier can be trained to be more sensitive in positive detection. The modification for weights updating is as following:

$$w_{t+1}(i) = \frac{w_t(i)}{z_t} \times \begin{cases} e^{-\alpha_t}, & h_t(x) = c_i \\ e^{\alpha_t}, & h_t(x) \neq c_i \end{cases} \tag{3}$$

$$z_t = \sum_i^T w_t(i) \times e^{\alpha_t \times (-1)^{\text{flag}}}, \quad \alpha_t = \frac{1}{2} \ln\left(\frac{1-\varepsilon_t}{\varepsilon_t}\right) + e^{p_t} \tag{4}$$

where z_t is the normalization factor, α_t is the weight factor, and p_t is the sum weight of all the correctly classified candidates in t round. The flag is equal to 0 when $h_t(x) \neq c_i$ is satisfied, otherwise the flag is equal to 1.

3. Performances and analysis

3.1. Dataset and evaluation methods

In order to detect small craters on Mars based on the modified algorithm, we choose the panchromatic image from the High Resolution Stereo Camera (HRSC) onboard Mars Express with a resolution of 12.5 m/pixel. One complete HRSC image contains hundreds of millions pixels, which is a really time-consuming work for mannual detection. Here four images from HRSC covering different areas are selected to test automatic detection performace of impact craters based on the modified algorithm. To correctly validate the detection results, we have mannualy selected these craters ranging from 300 m to 2500 m on these areas. We cannot detect craters as small as a few pixels without visual inspection, and the craters with diameter from 24 pixel to 200 pixel are reliably detected by this algorithm. The performance of our crater detection algorithm is evaluated by the framwork from Salamuniccar and Loncaric (2008b). The quality factors are normally utilized to evaluate our method (Shufelt, 1999). The computation of true detection rate(TDR) and false detection rate (FDR) is given by the followings:

$$\text{TDR}(\%) = \frac{TD}{GT} \times 100\% \tag{5}$$

$$\text{FDR}(\%) = \frac{FD}{TD+FD} \times 100\% \tag{6}$$

where TD is the number of true detection, GT is the total number of detected craters in the gound truth image and FD is the number of falsely detected craters. As our algorithm is a feature-based approach, which requires a number of pixels to constitute features within a image block. The smaller limit of the detected crater size is 24 pixel, and the largest detected craters is 200 pixel.

3.2. Performance and discussion

As an important indicator in the training process, the weighted classification error is a key factor to evaluate the performance of the weak classifier and make a difference in the process of updating weights. After applying the dual-threshold weak classifier instead of the single threshold one, the weighted classification errors have been degraded greatly (Fig. 3).

Fig. 4 shows the top 10 mask-features in the training phase with the modificated algorithm. All the features are ranked by the important factor α, which has correlation with the classification errors. We can select the minimum required number of features from the ranked features. Note that almost the top 10 features appear to focus on detecting the rim of the craters, which confirms our idea that the boundary between the light and shadow part of a crater is the most important feature for the detection of craters.
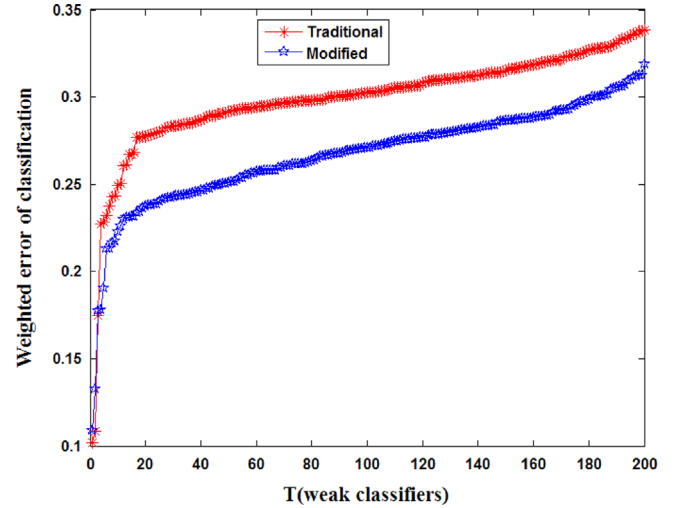

Fig. 3. The weighted classification errors.

When we set $\mu = 0.85$, the performances of the two approaches are shown in Fig. 5. The roughness of the surface really affects the detection results, which results in some missing detections and false detections. Furthermore, the consuming time from the improved method is also reduced a little.

By using the series of weak classifiers from the training set, we finaly build a strong classifier for the classification. The detections will be automatically evaluated as true or false craters by comparing with the manually built true results. There are 1055 ground truth craters in the selected areas for the test. By setting different thresholds, we can obtain the detection performance with comparing to the ground truth catalogue. It is clearly seen that the performance varies with the change of the threshold. When a lower threshold is determined in the classification, the higher true detection rate (TDR) and false detection rate (FDR) are obtained at the same time. It can be easily understood that a low threshold determines more obscure detections, including potential true detection and fase detection. The detection results show a better performance when compared to previous work. The detection rate of template matching (Bandeira et al., 2007), shape features analysis (Urbach and Stepinski, 2009), and Hough transform (Bue and Stepinski, 2007) are 86%, 70% and 64%, respectively. Obviously, the template matching method has the best TDR in these three methods. However, the false detection rate of template matching method is about 16%, and the modified method has higher TDR with about 90% if the FDR is close to 16%. To understand the relation between the threshold and detection rate, several different threshold values are chosen in the test. In Table 1, it has shown that both TDR and FDR fall with increasing the threshold value, but FDR has sharper decrease than TDR. When the FDR decreases from 40% to 10%, the TDR has only 12% decrease with still as high as 85%. At the same time, the modified method shows a better performance than the original method at different thresholds. Especially when the threshold value is set as 0.85, the TDR has an improvement of about 10% when compared to the original method, but no big change of the FDR. Obviously, the choice of the threshold value should be made according to the tradeoff between the TDR and FDR, which can be of good ability in the true detection of impact craters. We can improve the TDR when the modified approach is applied in the detection. Therefore, the modified algorithm has improved the performance of the crater detection.

The TDR has been significantly improved by 10%, while the FDR has less than about 2% change (Table 1), which confirms the effectiveness of the modified algorithm. However, some factors can contribute to a decrease of the TDR, such as the distribution of the sampling craters and homogenity of the test region. The weak link of this algorithm is the uncertainty of selecting crater candidates, which
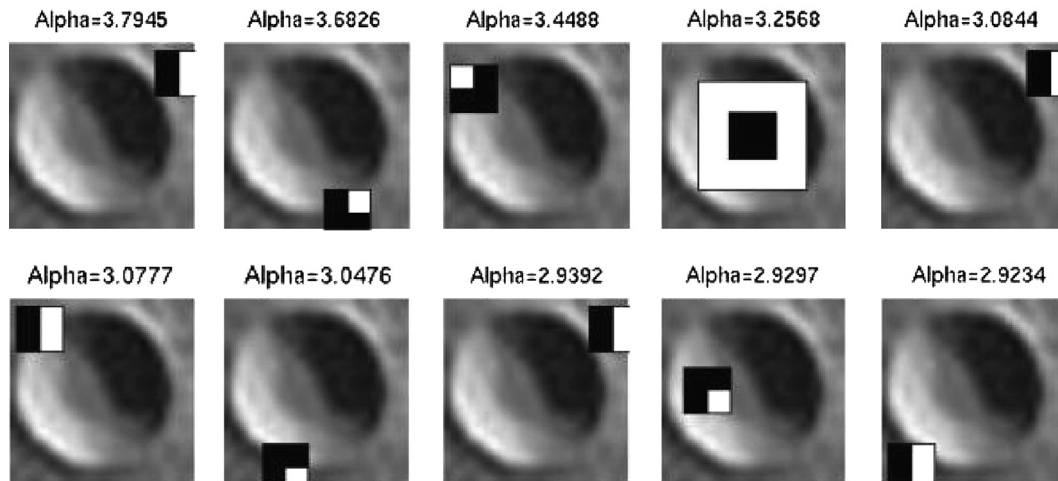
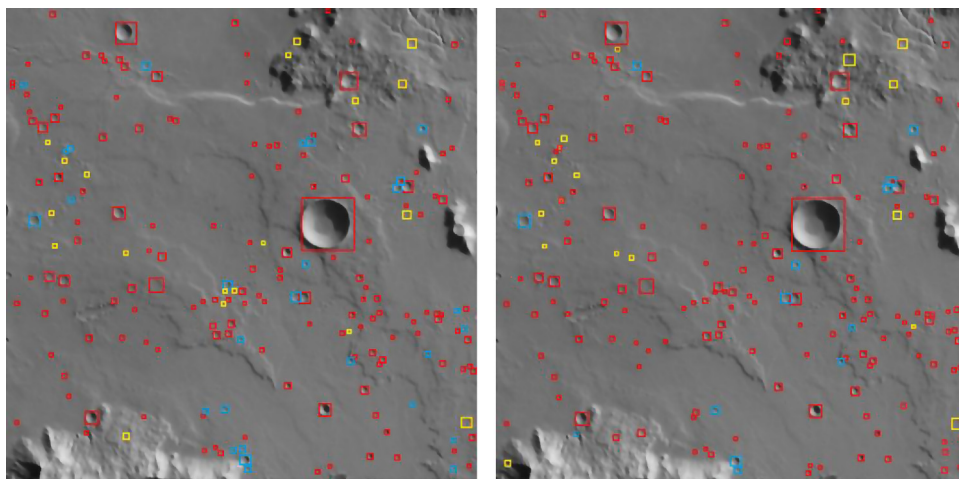**Fig. 4.** Top 10 mask-features selected in training phase with a dual-threshold.

Fig. 5. The red rectangles are true detections, blue ones are missing detections and yellow ones are false detections. The right picture is from the original method, and the left one is from the modified method. (For interpretation of the references to color in this figure legend, the reader is referred to the web version of this article.)

Table 1
Classification performance of the two approaches with different threshold values.

Threshold	Original method		Improved method	
	TDR (%)	FDR (%)	TDR (%)	FDR (%)
0.55	92.3	40.1	97.3	40.3
0.65	88.2	25.6	94.2	28.3
0.75	83.9	17.6	91.2	18.6
0.85	75.5	8.8	85.2	10.1

needs abundant samples to overcome it. If all ground truth craters are covered by the candidates, it can reduce the uncertainty but also consume more time. In addition, the realistic scenario of obtaining samples for the training set is from the spatially limited region, so the performance of the algorithm depends on the similarity of the crater candidates with the training set. In the future, the technique of transfer learning (Dai et al., 2007) will be further incorporated into the algorithm in the modification of the training set.

4. Conclusion

In this paper we present a modified algorithm to detect small-size craters on Mars. The dual-threshold weak classifier based on the characteristics of the feature value distribution is constructed instead of the single threshold classifier and the criterion of updating weights is adjusted in the process of training. The small craters on Mars are autamatically detected and tested based on the modified method using the images from the High Resolution Stereo Camera (HRSC) onboard Mars Express with a resolution of 12.5 m/pixel. Results show that the modified algorithm can improve performance in detecting small craters on Mars. A high threshold with 0.85 is determined, and the true detection rate of small size craters on Mars can be improved by almost 10%. Therefore, the modified adaboosting approach is effective to improve the performance of the small size crater detection and reduce the detection time. In the future, more data are needed to further test and analyze.

References

Andersson, L.B., Whitaker, B.A. NASA catalogue of lunar nomenclature, In: NASA Reference Publication 1097, 1982.

Bandeira, L., Ding, W., Stepinski, T.F., 2012. Detection of sub-kilometer craters in high resolution planetary images using shape and texture features. Adv. Space Res. 49 (1), 64–74.

Barlow, N.G., 1988. Crater size-frequency distributions and a revised Martian relative chronology. Icarus 75 (2), 285–305.

Bandeira, Saraiva, L.J., Pina, P., 2007. Impact crater recognition on Mars based on a probability volume created by template matching. IEEE Trans. Geosci. Remote Sens. 45 (12), 4008–4015.

Bue, B.D., Stepinski, T.F., 2007. Machine detection of Martian impact craters from digital topography data. IEEE Trans. Geosci. Remote Sens. 45 (1), 265–274.

Crater Analysis Techniques Working Group, 1979. Standard techniques for presentation and analysis of crater size-frequency data. Icarus 37, 467–474.

Ding, W., Stepinski, T., Mu, Y., Bandeira, L., Vilalta, R., Wu, Y., Lu, Z., Cao, T., Wu, X., 2011. Sub-kilometer crater discovery with boosting and transfer learning. ACM Trans. Intell. Syst. Technol. 2 (4), 39.

Dai, W., Yang, Q., Xue, G.-R., Yu, Y. Boosting for transfer learning. In: ICML'07: Proceedings of the 24th International Conference on Machine Learning. 2007, pp. 193–200.

Freund,Y., Schapire, R. 1995. A decision-theoretic generalization of on-line learning and an application to boosting. In: Proceedings of the European Conference on Computational Learning Theory (EuroCOLT). Springer-Verlag, 23-37.

Jin, S.G., Arivazhagan, S., Araki, H., 2013. New results and questions of lunar exploration from SELENE, Chang'E-1, Chandrayaan-1 and LRO/LCROSS. Adv. Space Res. 52 (2), 285–305, http://dx.doi.org/10.1016/j.asr.2012.11.022.

Kozlova, E.A., Michael, G.G., Rodinova, J.F., Shevchenko, V.V. Compilation and Preliminary Analysis of a Catalogue of Craters of Mercury. In: Lunar and Planetary Science XXXII (CD-ROM), Abs. 1231, 2001.

Kim, J.R., Muller, J.-P., Impact crater detection on optical images and DEMs. In: Proc. ISPRS, Houston, TX, 2003.

Leroy, B., Medioni, G.G., Johnson, E., Matthies, L., 2001. Crater detection for autonomous landing on asteroids. Image Vision Comput. 19 (11), 787–792.

Martins, R., Pina, P., Marques, J., Silveira, M., 2009. Crater detection by a boosting approach. IEEE Geosci. Remote Sens. Lett. 6, 127–131.

Papageorgiou, C., M. Oren, T. Poggio. 1998. A general framework for object detection. In: Sixth International Conference on Computer Vision, pp. 555–562.

Robbins, S.J., Hynek, B.M., 2012. A new global database of Mars impact craters ≥ 1 km: 1. Database creation, properties, and parameters. J. Geophys. Res.—Planets 117, E05004, http://dx.doi.org/10.1029/2011JE003966.

Rodionova, F.J., Dekchtyareva, K.I., Khramchikhin, A.A., Michael, G.G., Ajukov, S.V., Pugacheva, S.G., Shevchenko, V.V. Morphological catalogue of the craters of Mars. In: ESA-ESTEC, 2000.

Stepinski, T.F., Mendenhall, M.P., Bue, B.D., 2009. Machine cataloging of impact craters on Mars. Icarus 203 (1), 77–87.

Salamuniccar, G., Loncaric, S., 2008a. GT-57633 catalogue of Martian impact craters developed for evaluation of crater detection algorithms. Planet. Space Sci. 56 (15), 1992–2008, http://dx.doi.org/10.1016/j.pss.2008.09.010.

Salamuniccar, G., Loncaric, S., 2008b. Open framework for objective evaluation of crater detection algorithms with first test-field subsystem based on MOLA data. Adv. Space Res. 42 (1), 6–19.

Salamuniccar, G., Loncaric, S., 2012. Crater detection algorithms: a survey of the first decade of intensive research. In: Veress, B., Szigethy, J. (Eds.), Horizons in Earth Science Research, vol. 8. Nova Science Publishers, NY, USA, pp. 93–123.

Shufelt, J.A., 1999. Performance evaluation and analysis of monocular building extraction from aerial imagery. IEEE Trans. Pattern Anal. Mach. Intell. 21 (4), 311–326.

Tanaka, K.L., 1986. The stratigraphy of Mars. J. Geophys. Res. 91 (B13), 139–158.

Troglio, J., Le Moigne, J., Benediktsson, J., Moser, G., Serpico, S.S., 2012. Automatic extraction of ellipsoidal features for planetary image registration. IEEE Geosci. Remote Sens. Lett. 9 (1).

Urbach, Erik R., Stepinski, Tomasz F, 2009. Automatic detection of sub-km craters in high resolution planetary images. Planet. Space Sci. 57 (7), 880–887.

Viola, P., Jones, M.J., 2004. Robust real-time face detection. Int. J. Comput. Vision 57, 137–154.

Wetzler, P., Honda, R., Enke, B., Merline, W., Chapman, C., Burl, M. 2005. Learning to detect small impact craters. In: Proceedings of the Seventh IEEE Workshops on Application of Computer Vision. Vol. 1. pp. 178–184.